Check for updates

Collection of nectar by bumblebees: how the physics of fluid demonstrates the prominent role of the tongue's morphology

Amandine Lechantre,[a] Denis Michez[b] and Pascal Damman ⓘ *[a]

Bumblebees and some other tiny animals feed on nectar by visiting flowers in their neighborhood. Some bee species appear to be highly specialized, their tongue being adapted to specific flowers. *Bombus terrestris* in contrast is able to feed on a wide variety of flowers and can thus be considered as a kind of universal nectar catcher. Since plant nectars show highly variable sugar content, *Bombus terrestris* have developed a capture mechanism that works for almost any fluid viscosity. Their tongues are decorated with very elongated papillae forming a hairy coating surrounding a rod-like main stalk. When settled on a flower, *Bombus* rapidly dip their tongue into the inflorescence to catch the highly sought-after nectar. To determine the physical mechanism at the origin of this outstanding ability, the capture dynamics was followed from videos recorded during viscous fluid ingestion. Surprisingly, the volume per lap and the lapping frequency are independent of the fluid viscosity over three orders of magnitude. To explain this observation, we designed a physical model of viscous dipping with structured rods. Predictions of the model compared to observations for bees showed that the nectar is not captured with the help of viscous drag, as proposed in the Landau–Levich–Derjaguin model, but thanks to the hairy structure that traps the viscous fluid, capillary forces drastically limiting the drainage. Our approach can be transposed to others nectar foragers such as bats and hummingbirds.

1 Introduction

During evolution, various and sometimes surprising methods have been developed by animals to ingest liquids. A compendium of drinking strategies encountered in the animal realm is compiled in the review of Kim and Bush.[1] They emphasize that animals adapt their method to their size and the properties of the fluid to be ingested. Gravitational, viscous, capillary, and inertial forces thus balance to determine the rate and volume of the captured fluid. For most insects and other tiny animals, beyond the action of muscles, capillary and viscous forces are dominant. Interestingly, viscous forces both facilitate fluid capture (*e.g.*, drag in viscous dipping) and hinder it (*e.g.*, dissipation in capillary filling of tubes). While viscosity of water is relatively low, plant secretions like nectar can show high viscosity challenging the food intake strategy of the floral visitors (*e.g.*, bees visit flowers producing nectar from 0.001 to 0.5 Pa s).[2–4] In addition, the viscosity of plant secretions can exhibit large variations during the same day, depending on weather conditions.

The collection of nectar can be seen as a simple energy supply taking advantage of the high sugar fraction contained in these plant secretions. Its optimization should maximise the energy-intake rate $\dot{E}$ defined by the product of the energy content per unit mass of sugar, ε, the density ρ of the nectar, the volumetric fraction of sugar in nectar C and the volumetric flow rate Q by the relation $\dot{E} = \varepsilon\rho CQ$.[5] While ε and ρ can be considered as constants (small variations related to chemical composition and concentration can however be observed even within the same flower species), C and Q strongly depend on the viscosity of the nectar. This viscosity exponentially increases with the sugar concentration at a given temperature and also depends on the exact composition of the nectar (the ratio of different types of sugar contained in the nectar but also the presence of various compounds such as amino acids or enzymes).[3] To optimize $\dot{E}$, animals should then both maximize the sugar content C and the flow rate Q. The sugar content C is determined by the type of flower visited, a tremendously relevant parameter but completely fixed by the characteristics of the foraging area. From the physical point of view, the only adjustable parameter is Q. This important parameter could be adapted by both the shape and the kinematics of the tongue. Careful analysis of these relationships could ultimately give a strong support to the idea that evolution has selected the species optimizing

[a] Laboratoire Interfaces & Fluides Complexes, Université de Mons, 20 Place du Parc, B-7000 Mons, Belgium. E-mail: pascal.damman@umons.ac.be

[b] Institut des Biosciences, Laboratoire de Zoologie, Université de Mons, 20 Place du parc, 7000 Mons, Belgium

the capture of nectar in a given region and/or a given group of plants.

Kim *et al.* proposed two main mechanisms to describe the capture of nectar by various animals, including bees, hummingbirds, butterflies, and bats. The first one is related to suction by the action of capillary forces or muscles, and the second one is based on viscous dipping.[1,6] To theoretically estimate the evolution of ingestion rates with nectar viscosities, they proposed a reasonable hypothesis: the animals capture the fluid with a constant power. This assumption yields scaling laws for the flow rates (*i.e.*, $Q \propto \eta^{-1/2}$ for suction and $Q \propto \eta^{-1/6}$ for viscous dipping, η being the nectar viscosity), that qualitatively fit the compiled experimental data found in the literature.[6] It should be noted however that the leading hypothesis of constant retraction power is not supported by any experimental observations in the literature. Last but not least, they assimilated animal tongues to simple tubes or smooth rods, the micro-structures such as hairy papillae, that decorate the tongues of bees and bats, being discarded. More recent works suggest however that the capture of nectar depends on the morphology and the dynamics of the tongue. Yan *et al.* proposed a mechanism of capture based on a very complex coordinated dynamics between the back and forth movement of the tongue in the fluid coupled to the erection of the hairy papillae coating the tongue.[7–12] In summary, while several works in the literature discuss the capture of nectar by bees, the true influence of the micro-structures of the tongue is still questionable and a physical model describing quantitatively the fluid capture by nectarivores remains to be designed.

In this paper, we will address these specific problems by studying in detail the collection of nectar by a single species, *Bombus terrestris*. The studied species has been chosen for its polylectic character, *i.e.*, bees that collect nectar and pollen from flowers of a variety of unrelated plants.[13] The advantage of focusing the study on a non-specialized species is to avoid exotic tongue morphologies resulting from a specific co-evolution of flowers and bees.[14] Our study is based on the analysis of videos of bumblebees ingesting nectars of various viscosities and a detailed physical study of the viscous dipping for smooth and structured rods. The quantitative comparison of biological data with predictions of the physical model should help to derive a novel perspective about nectar capture.

2 Experimental section

Bumblebees

We study *Bombus terrestris audax*. The worker bumblebees come from a colony bought from Biobest firm (Westerlo, Belgium). The colony was kept at the temperature of 27 °C and humidity of 65–70%.[15] They were fed every two days with pollen candies and a sweet solution imitating nectar (Biogluc pink) was provided to them *ad libitum*.

Video recording of nectar capture

The experimental setup for observing the drinking process is based on a previously reported protocol[16]: before beginning the observation of the drinking process, bumblebees were starved

at room temperature in the dark from 2 to 4 hours. Then, a bumblebee was transferred into the holding tube which is a 15 mL centrifuge tube with a 4 mm hole at the tip (Fig. 1B). After a habituation phase of 3 minutes, the extension of the proboscis is motivated by presenting a drop of a solution of diluted honey. Finally, a capillary tube with a sweet solution of known viscosity (from 10^{-3} to 0.3 Pa s) is presented to the bumblebee. The experiments are filmed using a camera Logitech C920, at up to 30 frames per second.

Physical model of the viscous dipping process

During experiments performed on smooth rods of diameter d (1 mm $< d <$ 6.9 mm) and on structured rods, the thickness of the dragged fluid was followed over time *via* the measurement of the total mass of the fluid entrained on the rod. Fluids (silicon oil) of viscosity, η, of 0.5, 1 and 5 Pa s were tested with withdrawal rates between 1 and 40 mm s^{-1}. The structured rods have been made by 3D printing by the company, Sculpteo. The internal diameter, R_i, the gap between pillars, D, depth of the structure, H, and thickness of a ridge, d, of the different structures are compiled in Table 1.

3 Results and discussion

Dynamics of nectar capture

To validate a physical model relating the nectar flow rate to the bumblebee's tongue characteristics, we need relevant values of ingestion rates Q, determining the energy-intake rates. For this purpose, we recorded videos of bumblebees (*Bombus terrestris*) capturing artificial nectars with different sugar contents, *i.e.*, different viscosities (see Experimental section for details). The fluid is contained in a capillary tube of 1 mm diameter (Fig. 1B). The evolution of the meniscus with time (Fig. 1C) reveals small periodic variations related to the periodic movement of the tongue. After a short adaptation time, the curves become very regular, both in time and volume (with deviations less than 20%). Analysis of the meniscus displacement yields the average lapping rate ν and the average captured volume for each lap v_0 for different nectar viscosities spanning three orders of magnitude (Fig. 1D). From these data, the ingestion rate $Q \sim \nu v_0$ can be computed. Counterintuitively, the ingestion rate does not depend upon the fluid viscosity (Fig. 1E). The velocity of the tongue and the ingestion rate are thus not determined by the viscosity. These observations contradict the constant power output hypothesis based on the first proposed model,[6] with $Q \propto \eta^{-1/6}$. These authors consider that, whatever the viscosity is, the work per unit time required to overcome the viscous friction, or equivalently the power output is constant. For clarity, we briefly recall the main process of the previous analysis. The muscular power required to overcome the viscous drag should be given by $\dot{W} \sim \eta V^2 L$, where V and L are respectively the velocity and the length of the tongue. Considering that a constant power output leads to a decrease in the lapping rate with viscosity according to the $\nu \sim V/L \propto \eta^{-1/2}$ power law.[6] Instead, our experiments show that the lapping rate is found to
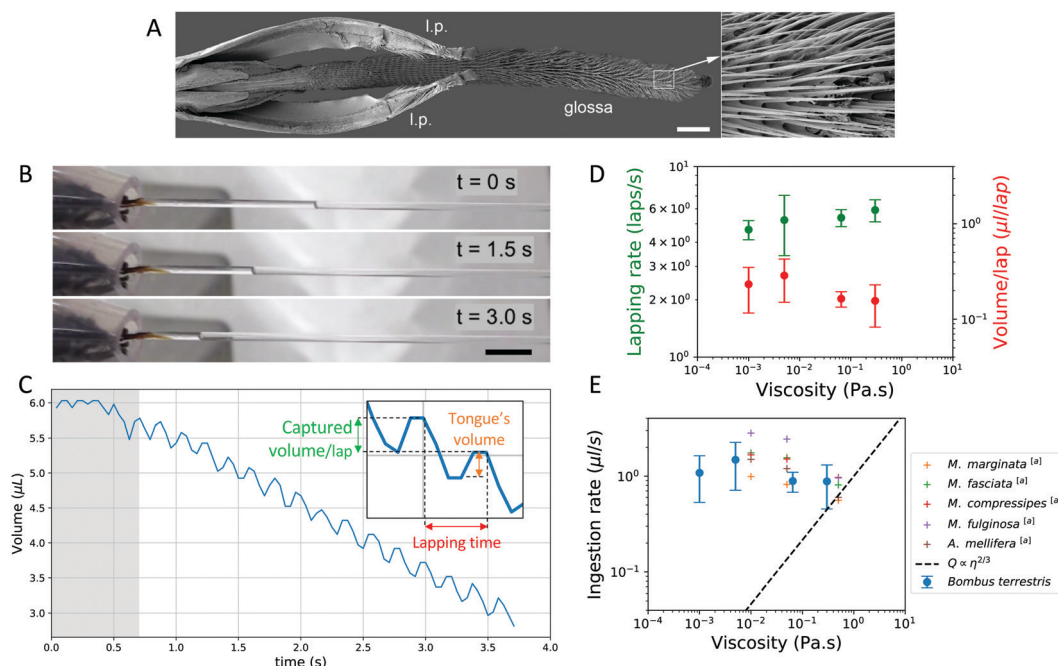
Fig. 1 (A) Glossa and labial palpae (l.p.) of *Bombus terrestris* with a detailed setae structure (scale bar: 400 μm). (B) Time sequence images of the collection of nectar by a bumblebee. The bumblebee is maintained in an open holding tube placed close to a capillary tube of 1 mm diameter containing the sugary solution. The evolution of the position of the meniscus on the capillary tube allows us to determine the quantity of the captured solution (scale bar: 5 mm). (C) Evolution of the volume of the solution with time in the capillary tube. The inset shows a close-up of the same graph. (D) Lapping rate (in green) and captured volume by lap (in red) for different fluid viscosities (4 to 7 bees for each viscosity). (E) The ingestion rate for different viscosities. Our measurements correspond to the blue dots. Data from the literature appear as crosses.[4] The dashed black line represents the evolution of the ingestion rate following the LLD law calculated with a constant lapping rate.

Table 1 Dimensions of the structures. R_i, d, D and H represent the inner diameter of the rod, the width of a pillar, the gap between pillars and the depth of the microstructure, respectively. All lengths are given in mm

Name	R_i	D	H	d
A	4.82	1.2	1.2	1.2
B	4.82	1.6	1.2	1.2
C	4.82	2.4	1.2	1.2
D	4.82	1.2	1.6	1.2
E	4.82	1.2	2.4	1.2
F	4.82	1.2	4.8	1.2
G	4.82	1.2	1.2	1.6
H	4.82	1.2	1.2	2.0
I	4.82	1.2	1.2	2.4

be constant for a very large range of viscosities. It should be noted that our data are in close agreement with those previously reported in the literature.[4]

The logical consequence of this observation is rather unexpected. It clearly indicates that, during a short period of adaptation lasting less than 1 s (the grey zone in Fig. 1C), the bumblebees are able to adjust the retraction force to the viscosity of the nectar. Such an adaptive behavior is supported by a previous study showing that bees prefer warmer and less viscous nectar, regardless of the sugar concentration.[17] Hummingbirds have a sweet taste perception[18] but this observation suggests that bumblebees have a viscosity perception. Moreover high learning abilities have already been proven for honey bees and bumblebees.[19,20] This raises a

fundamental question: what determines the lapping frequency, if it is not the muscle power? We could only suggest a hypothesis. For instance, limiting the captured nectar volume below the maximum amount they can swallow is an issue of survival.[21]

As a first try, we amended the model previously proposed by Kim *et al.*[6] by replacing the constant power assumption by the observed constant lapping rate. As they suggested, the volume of nectar per lap can be estimated by considering the Landau–Levich–Derjaguin, LLD, mechanism.[22,23] The thickness of fluid dragged during retraction is determined by the bees tongue radius R and the capillary number, Ca = $(\eta V/\gamma)$ through the relation $h \sim R\text{Ca}^{2/3} \sim R(\eta V/\gamma)^{2/3}$, which suggests that the ingestion rate follows $Q \sim RhV \propto \eta^{2/3}$. As shown in Fig. 1E, this law is in complete contradiction with the observed constant volume per lap, lapping rate and ingestion rate. Neither the independence with the viscosity nor the absolute values of Q, much higher than the predictions, are compatible with this model.

Thus, how could we explain the constant volume per lap for viscosities spanning three orders of magnitude? The severe inconsistency of the previous model clearly suggests that we should discard the proposed LLD hypothesis and test other processes. In the following, we build a physical model of viscous dipping taking into account the influence of the micro-structures that decorate the bumblebees' tongue (Fig. 1A).

Viscous dipping with micro-structured rods

Considering the shape of the tongue (*i.e.*, a stalk coated with sub-millimetric hairy papillae), the collection of nectar by bumblebees can be mimicked as the dipping of thin rods decorated with regular micro-structures in a fluid of controlled viscosity. A few works were devoted to the influence of micro-structures on the viscous dipping with plates.[24–26] From the study of sanded glass plates, Krechetnikov *et al.* showed that depending on the roughness σ_R and the thickness of the fluid film h, three regimes can be defined: (i) for $\sigma_R \ll h$, the roughness does not produce any observable effect and can be neglected, (ii) for $\sigma_R \gg h$, the liquid essentially fills the cavities, the fluid thickness becomes independent of Ca (drag becomes negligible), and (iii) the intermediate regime, $\sigma_R \sim h$, where both contributions are comparable. The fluid flow at the rough interface is perturbed and can be described by considering a slippage length at the solid–fluid interface.[24] Seiwert *et al.* extensively studied viscous dipping with silicon wafers decorated with regular arrays of micrometric pillars.[25] They also observed the three regimes first proposed by Krechetnikov, and suggest a model with two viscosities. In fact, the flow within the forest of pillars, that could be related to a wicking of the micro-structure, is replaced in the model by a layer of very large viscosity. They suggest that it is possible to consider separately the contributions from the roughness and from the drag, $h(\text{Ca}) = h_0 + h_{\text{drag}}(\text{Ca})$. More recently, Nasto *et al.* reported the viscous dipping of plates coated with regular arrays of millimetric pillars. They showed that, for the studied range of experimental parameters, the final amount of dragged fluid is essentially determined by the drainage dynamics of the fluid trapped in the microstructure during the retraction time.[26]

Unfortunately, none of these studies investigate experimental conditions close to those estimated for the capture of nectar by bumblebees, *i.e.*, large capillary numbers, $0.01 < \text{Ca} < 1$ and a rod-like geometry with submillimetric decorations.[3,4] Studies reported by Krechetnikov *et al.*[24] and Seiwert *et al.*[25] focused on plates and very small capillary numbers, $\text{Ca} < 10^{-2}$. Nasto *et al.* described the drainage of plates coated with large millimetric pillars.[26] The micro-structures on the tongue of *Bombus terrestris* are only spaced 20 µm apart (Fig. 1A), much smaller than the capillary length. In this case, capillary forces prevent any fluid drainage from the structure. We thus investigate viscous dipping with structures trying to mimic bee's tongues. Unfortunately, the hairy structure formed by an array of very elongated papillae is very difficult to produce by 3D printing. Instead we chose to use simpler shapes, reminiscent of honey spoons, *i.e.*, rods of finite length, different radius and decorated with a periodic structure of valleys and ridges, keeping a radial symmetry. At first sight, these micro-structured rods seem to be far from the hairy structures observed in bumblebees but they appear to be helpful to derive the general rules governing the capture of fluid by rods of complex shapes.

Smooth rods. First, we study fluid capture with smooth rods to investigate the influence of the radius. As shown in Fig. 2A and B, the withdrawal of a rod immersed in a viscous fluid involves the drag of fluid immediately followed by a drainage process.

For ease of comparison with the theory, the measured mass of fluid is converted into thickness, through the relation $M \sim \rho R h L$ with R the radius of the rod and L the immersed distance. As previously shown, the dynamics of drainage are determined by a balance of gravity, *i.e.*, the driving force, with a dissipative force dominated by the viscous flow in the dragged fluid layer. As shown in Fig. 2C, it is adequately described by the scaling relation, $h/l_c \sim (\eta L/\gamma)^{1/2} t^{-1/2}$, (with the capillary length $l_c = (\gamma/\rho g)^{1/2}$), obtained by considering volume conservation and the Stokes equation.[27,28]

When considering the collection of fluid by animals, the most relevant parameter is the maximum amount of nectar that could be obtained per lap. In Fig. 2D, the maximum fluid thickness computed from the mass at maximum is plotted *versus* the capillary number for various radii. The data reported by Seiwert *et al.*[29] and Maleki *et al.*[30] for the viscous dipping of plates at low capillary numbers ($\text{Ca} < 0.1$) were added for clarity. For plates, previous studies showed that the evolution of fluid thickness with Ca can be described by two asymptotic regimes. At low Ca, the LLD relationship $h \sim l_c \text{Ca}^{2/3}$ fully determines the thickness.[22] Above a critical capillary number $\text{Ca}^\star$, a transition towards a gravity dominated regime characterized by the relation $h \propto \text{Ca}^{1/2}$ is observed.[23] For rods, the situation is slightly more complex. At low Ca, all data for plates and rods collapse on a single master curve. For a high Ca, however, the fluid thicknesses measured for various rods collapse on two different curves, depending on their radius. For thin rods, $R < l_c$, the fluid thickness follows the classical $h \propto \text{Ca}^{2/3}$ LLD relationship. For thick rods, $R > l_c$, the rods behave in the same way as plates, with a transition towards a gravity dominated regime with $h \propto \text{Ca}^{1/2}$. The occurence of two regimes for the same range of Ca can be rationalized by considering the change of the relevant length-scale, l_c *vs.* R. Thick rods, $R > l_c$, can be considered as plates. We thus have to explain: (i) the transition from capillary to gravity dominated regimes observed for plates and thick rods, and (ii) the disappearance of this transition for thin rods.

The transition between two asymptotic behaviors at a critical capillary number was previously reported for plates,[23] and corresponds to a switch from Laplace pressure dominated to hydrostatic dominated regimes. The difference in dynamics results from a change in the pressure gradient term in the Stokes equation, $\eta \nabla^2 V = \nabla P$. In the capillary regime, $\nabla P \sim \gamma \kappa / \ell$, where κ, and ℓ are the curvature of the static meniscus and the length of the dynamic meniscus, respectively. The assumption that dynamic curvature should be equal to the static one, $\kappa \sim 1/l_c \sim h/\ell^2$, finally gives the LLD relationship $h \sim l_c \text{Ca}^{2/3}$. In the gravity dominated regime, also called the Derjaguin regime,[31] $\nabla P \sim \rho g$ which immediately gives the relation $h \sim l_c \text{Ca}^{1/2}$. The gravity regime appears when $\rho g \ell > \gamma/l_c$, *i.e.* when $\text{Ca} > 1$ in agreement with our observations for thick rods (Fig. 2D).

The disappearance of the transition for thin rods can also be rationalized from the derivation of the LLD model. For rods, there are two limiting cases for defining the mean curvature: (i) $\kappa \simeq 1/R$ which yields the relation $h \sim R\text{Ca}^{2/3}$, this corresponds to the rod-like regime; or (ii) $\kappa \simeq 1/l_c$, giving the relation
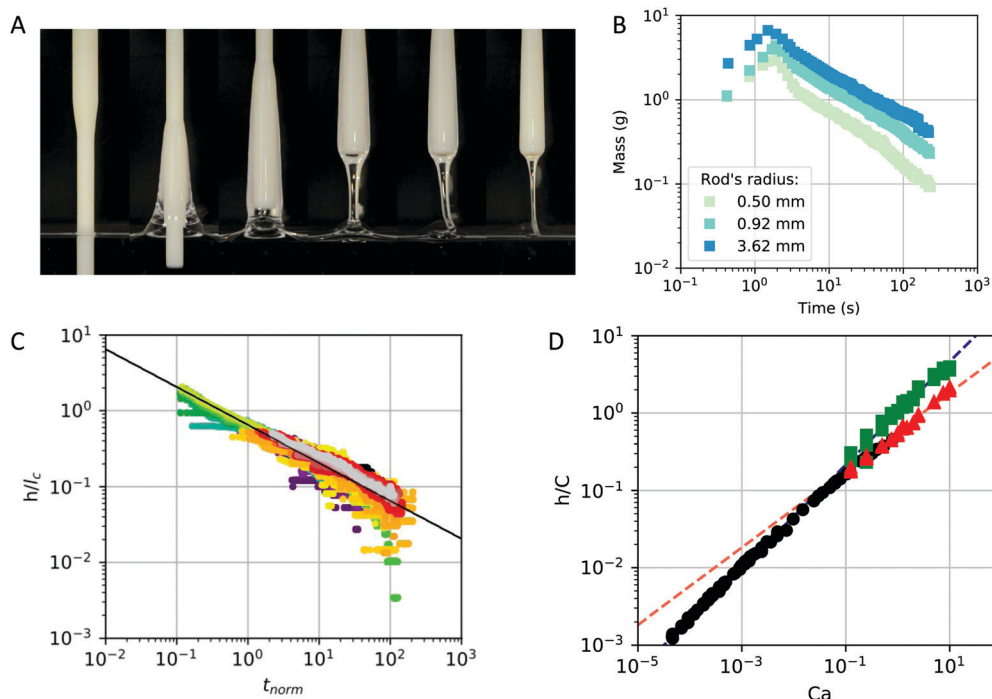
Fig. 2 (A) Image sequence recorded during the withdrawal of a smooth rod (R = 2.41 mm, η = 5 Pa s and V = 40 mm s^{-1}). (B) Evolution of the mass of dragged fluid over time. (C) Time evolution of the normalized thickness of the dragged fluid during the drainage stage (normalized time t_{norm} = ($t\gamma/L\eta$) where γ, L and η, are the surface tension, the immersed length and the fluid viscosity, respectively). The solid line represents the $t^{-1/2}$ power law. (D) Evolution of the normalized maximal thickness of the collected fluid with the capillary number, Ca (C is equal to l_c/R for thick/thin rods). Green squares: thin rods ($R < l_c$); red triangles: thick rods ($R > l_c$) and black circles: previously reported data for plates.[29,30] The red and blue dashed lines represent slopes of 2/3 and 1/2, respectively.

$h \sim l_c \mathrm{Ca}^{2/3}$, we name this regime plate-like. The transition between these two-regimes corresponds to $R \simeq l_c$. For thin rods, the Ca$^{1/2}$ gravity regime appears only when $\rho g \ell > \gamma/R$. This condition requires that Ca > Ca$^\star \sim (l_c/R)^6$. In most cases, this condition cannot be fulfilled and this regime is not observed (for instance, it should appear for Ca > 200 for the thin rods used here).

Structured rods. For studying the influence of the micro-structure, we used thick rods corresponding to the visco-gravitational regime, $h \propto \mathrm{Ca}^{1/2}$. While keeping a radial symmetry, various sizes of micro-structures were used, they are summarized in Table 1. The most obvious difference observed with structured rods with respect to their smooth counterparts appears during the drainage (Fig. 3B). The drainage dynamic does not follow anymore the $t^{-1/2}$ power law but instead asymptotically tends toward a constant value characterized by the size and geometry of the rod. This tendency can be related to the fluid trapped in the micro-structure by capillary forces that cannot be drained.

The presence of micro-structures on the rods raises several fundamental questions regarding the capture of the viscous fluid: how to quantitatively analyse the viscous drag for such heterogeneous system; how to define the thickness of the dragged fluid; and what the influence of valleys and ridges is on viscous forces.

Unfortunately, there is no obvious way to analyse the amount of fluid collected through viscous drag for such complex shapes.

Nevertheless, to be consistent with the results obtained for smooth rods, we choose to convert the mass of the fluid into an effective thickness, defined by the relation $M \sim \rho R_i L h_{eff}$, where R_i is the internal radius of the structured rod and L is the immersed distance. Interestingly, this effective thickness takes into account both the depth and density of ridges/valleys within a single parameter. The relevance of this particular choice will become clear later. The evolution of the effective thickness with the capillary number, Fig. 3C, shows drastic deviations with respect to smooth rods. Instead of a master plot with all curves collapsing, well-separated curves are observed for different structures. To rationalize these seemingly disparate curves, we follow a previously reported methodology [24,25] and estimate the thickness from two contributions: (i) the first one is related to fluid trapped in the micro-structure, h_0; (ii) the second contribution arises from the fluid carried away by the viscous drag, h_{drag}. As suggested by Kretchnikov,[24] this procedure, consisting in compiling two asymptotic behaviors, is relevant considering the global evolution of the effective thickness with Ca. For small Ca, the viscous forces are negligible, only the fluid trapped in the structures is carried away and the thickness is independent of Ca. For large Ca, the viscous forces become so large that we can neglect the trapped fluid; the curves become closer to the $h/l_c \sim \mathrm{Ca}^{1/2}$ law observed for smooth rods. The effective thickness of the fluid wrapped around the rod should then be given by, $h_{eff} = h_0 + h_{drag}$ where h_0 depends on the size and geometry of the micro-structure. To test this model,

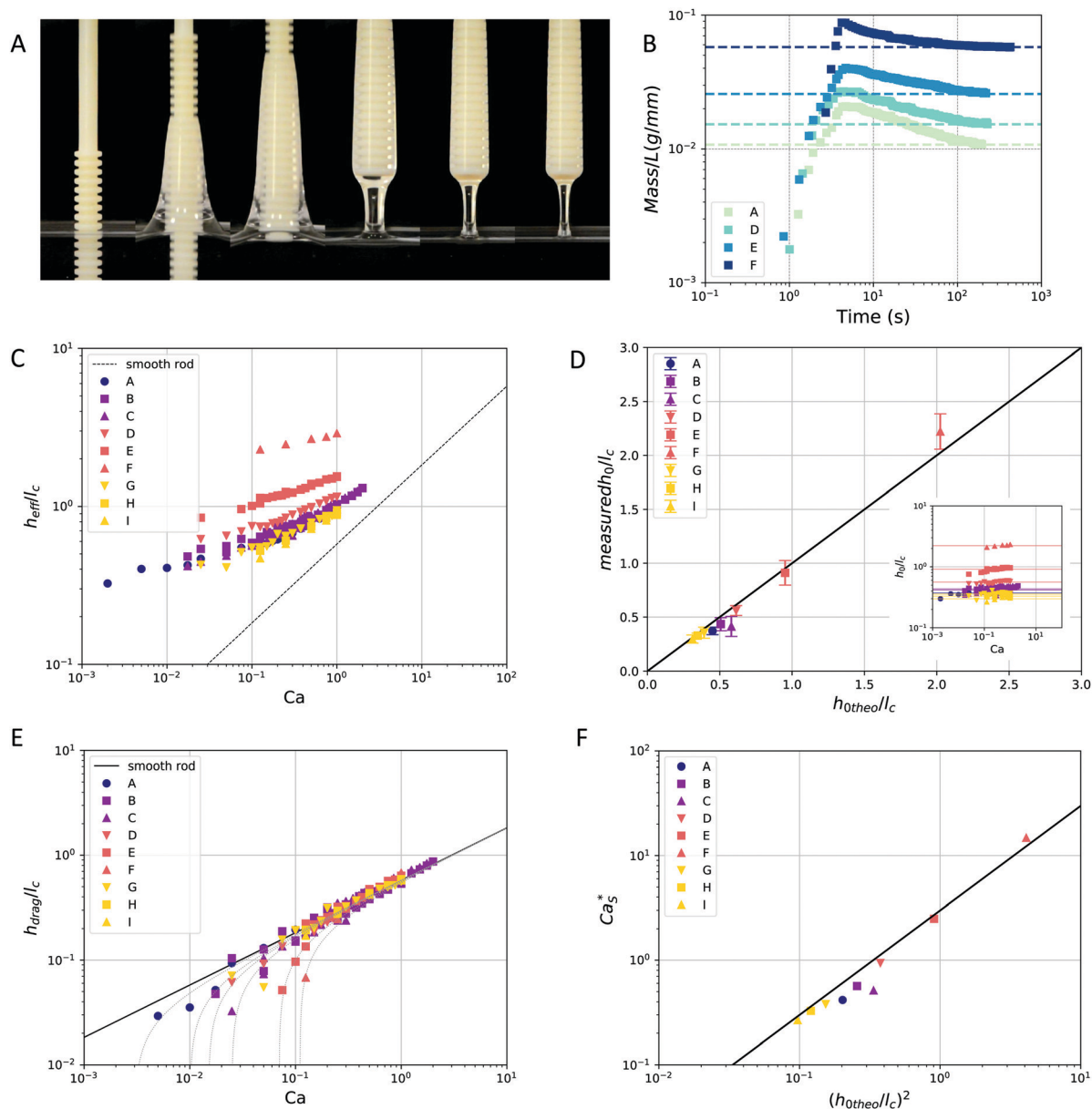Fig. 3 (A) Ssequence of images recorded during the withdrawal of a structured rod ('A' rod, R_i = 2.41 mm, h = d = D = 1.2 mm), η = 5 Pa s and V = 40 mm s^{-1}. (B) Time evolution for mass of captured fluid per immersed length unit. (C) Evolution of the effective thickness of the collected fluid with the capillary number. The dotted black line represents the data observed for smooth thick rods. (D) Comparison of measured and calculated trapped fluid h_0. Inset: Evolution of h_0 with Ca for different structures. (E) Plot of the dragged thickness contribution h_{drag} with the capillary number. Dotted lines represent theoretical predictions for structured rods. The solid line corresponds to smooth rods. (F) Plot of the measured critical capillary number Ca$_S$* versus the calculated value $(h_{0theo}/l_c)^2$ (see text).

we measure h_0 from raw data by eliminating the dynamic part of the thickness, through the relation $h_0 = h_{eff} - l_cCa^{1/2}$. As shown in Fig. 3D, the measured trapped fluid thickness is in agreement with the h_0 estimated from the geometrical characteristics of the micro-structures, $h_{0theo} = h(d/(D + d))$. Conversely, the contribution related to the viscous drag, h_{drag}, can be obtained from h_{eff} by subtracting the trapped fluid thickness, h_0. Fig. 3E shows that the fluid carried away by the viscous forces for these structured rods follows quantitatively the same law as smooth rods, $h/l_c \sim Ca^{1/2}$. However, when approaching a critical capillary number, Ca$_S$*, the contribution related to the viscous drag

vanishes as illustrated by drastic deviations observed at low Ca for the curves of Fig. 3E. This critical capillary number Ca$_S$* associated with the transition from trapped to viscous dominated regimes can be defined by considering $h_0 = h_{drag}$, which yields Ca$_S$* $\sim (h_0/l_c)^2$. The agreement between measured and calculated Ca$_S$* gives additional support to the proposed separation of the contribution to describe the fluid drag of structured rods (Fig. 3F). It should also be noted that there are no flow perturbations related to any interfacial slippage due to the structures detected in the measurements. Considering previous studies,[24,25,32] this can be explained by considering that (i) in
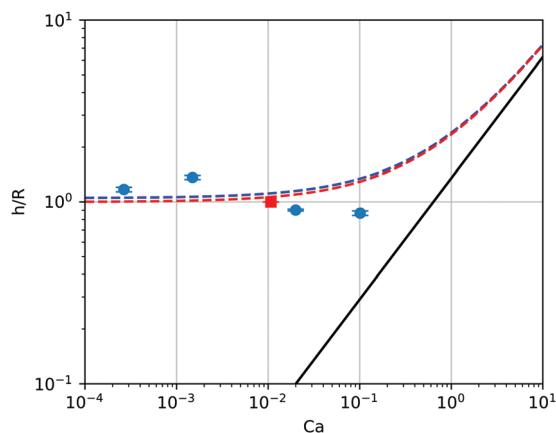
Fig. 4 Evolution of normalized thickness of nectar collected by bumblebees (blue circles) or bats (red circles, data reported in ref. 34) with the capillary number. The black solid line corresponds to the law expected for smooth rods ($R = 0.1$ mm) and the dashed lines represent the predictions of the new model for bumblebees (blue) or bats (red).

contrast to previous works on arrays of pillars, the fluid here is completely trapped in the structures (due to the "honey spoon" shape of the rods); (ii) the observed fluid thicknesses are millimetric and probably larger than the slippage length.

Application of the model to bumblebees

The proposed physical model based on structured rods could be easily transposed to bumblebees to get the volume per lap ($v_0 \sim RLh$, where R and L are the radius and length of the tongue, respectively). Fig. 4 shows the evolution of the effective thickness of the captured nectar with the capillary number. To apply the model to bumblebees, we should first determine the corresponding regime (gravitational *vs.* capillary and trapped *vs.* drag) by comparing the capillary numbers to the critical ones. Regarding the transition between capillarity and gravity dominated regimes, the tongue of the studied bumblebees corresponds to a thin rod, $R \simeq 0.1$ mm, decorated with flexible papillae of length, $h_0 \simeq 0.15$ mm. Firstly, these data yield very large critical capillary number, $Ca^* \sim (l_c/R)^6 = 10^6$. Bumblebees thus always collect the nectar in the capillary dominated regime. Secondly, we have shown that a transition from trapped to viscous dominated regimes appears for a critical capillary number. Its expression must be adapted to the bumblebees' characteristics. Considering that $h_0 = h_{drag} \sim RCa^{2/3}$, we obtain $Ca_S^* \sim (h_0/R)^{3/2} \simeq 1.9$. As the operating range of capillary numbers for bumblebees is between $10^{-2} < Ca < 0.1$, we could assume that the collected nectar is essentially located in the micro-structure, the amount of nectar taken by the viscous drag being negligible. As shown in Fig. 4, the predictions of the physical model are quantitatively in agreement with the values measured for living bumblebees without any fitting parameter. Finally, the trapping of the nectar within the papillae is only the first stage of collection of nectar by bumblebees. Once the tongue is filled with nectar and retracts, the nectar is unloaded in a tube formed by labial palpae (Fig. 1A). The loaded tongue is squeezed by labial palpae acting like a wedge and the nectar is

sucked into the mouth by the action of the pharyngeal pump.[33] The collection of nectar for bumblebees can be viewed as a "mopping-squeezing" mechanism.

4 Conclusions

In conclusions, this study gives a new insight into the interaction of viscous fluid with structured solid objects. We have rationalized viscous dipping under unexplored experimental conditions, *i.e.* millimetric rods decorated with micro-structures of radial symmetry. The assumption that it is safe to describe the dragged fluid with two independent contributions: one related to the fluid trapped in the micro-structure, and the other from the fluid carried away by the viscous drag, is validated from our experiments. Regarding the behavior of bumblebees, in contrast to previous studies, this quantitative work demonstrates that viscous dipping (dark line in Fig. 4) is not the dominant mechanism used by bumblebees to capture nectar. This clearly justifies the evolutionary purpose of the hairy micro-structure of papillae found at the tip of the tongue of many bees (Fig. 1A). Finally, the proposed physical model could probably be adapted for other animal species. For instance, some bats also capture nectar by using erectile papillae forming a hairy structured tongue. As we can see in Fig. 4, the predictions of the proposed model are compatible with the thickness of the dragged nectar measured for bats.[34]

Conflicts of interest

There are no conflicts to declare.

Acknowledgements

Notes and references

1 W. Kim and J. W. M. Bush, *J. Fluid Mech.*, 2012, **705**, 7–25.
2 M. S. Percival, *New Phytol.*, 1961, **60**, 235–281.
3 L. D. Harder, *Oecologia*, 1986, **69**, 309–315.
4 D. W. Roubik and S. L. Buchmann, *Oecologia*, 1984, **61**, 1–10.
5 J. G. Kingsolver and T. L. Daniel, *J. Theor. Biol.*, 1979, **76**, 167–179.
6 W. Kim, T. Gilet and J. W. M. Bush, *PNAS*, 2011, **108**, 16618–16621.
7 H. Yang, J. Wu and S. Yan, *Appl. Phys. Lett.*, 2014, **104**, 1–4.

8 J. Chen, J. Wu and S. Yan, *J. Insect Sci.*, 2015, **15**, 1–5.

9 C. Zhao, J. Wu and S. Yan, *J. Appl. Phys.*, 2015, **118**, 1–7.

10 J. Wu, R. Zhu, S. Yan and Y. Yang, *J. Exp. Biol.*, 2015, **218**, 664–667.

11 R. Zhu, H. Lv, T. Liu, Y. Yang, J. Wu and S. Yan, *J. Insect Behav.*, 2016, **29**, 325–339.

12 Y. Yang, J. Wu, R. Zhu, C. Li and S. Yan, *J. Bionic Eng.*, 2017, **14**, 607–615.

13 P. Rasmont, A. Coppée, D. Michez and T. De Meulemeester, *Ann. Soc. Entomol. Fr.*, 2008, **44**, 243–250.

14 A. Müller, *Eur. J. Entomol.*, 2006, **103**, 497–500.

15 H. H. Velthuis and A. van Doorn, *Apidologie*, 2006, **37**, 421–451.

16 C. Ma, S. Kessler, A. Simpson and G. Wright, *J. Visualized Exp.*, 2016, **113**, 1–7.

17 S. W. Nicolson, L. de Veer, A. Köhler and C. W. W. Pirk, *Proc. R. Soc. B*, 2013, **280**, 20131597.

18 M. W. Baldwin, Y. Toda, T. Nakagita, M. J. O'Connell, K. C. Klasing, T. Misaka, S. V. Edwards and S. D. Liberles, *Science*, 2014, **345**, 929–933.

19 R. Dukas and L. A. Real, *Anim. Behav.*, 1993, **45**, 37–41.

20 D. F. Sherry and C. G. Strang, *Behav. Processes*, 2015, **117**, 59–69.

21 J. H. Fewell and M. L. Winston, *Behav. Ecol.*, 1995, **7**, 286–291.

22 L. Landau and B. Levich, *Acta Physicochim. URSS*, 1942, **17**, 141–153.

23 A. de Ryck and D. Quéré, *J. Colloid Interface Sci.*, 1998, **203**, 278–285.

24 R. Krechetnikov and G. M. Homsy, *Phys. Fluids*, 2005, **17**, 102108.

25 J. Seiwert, C. Clanet and D. Quéré, *J. Fluid Mech.*, 2011, **669**, 55–63.

26 A. Nasto, P. T. Brun and A. E. Hosoi, *J. Colloid Interface Sci.*, 1998, **203**, 278–285.

27 A. Herczynski, C. Cernuschi and L. Mahadevan, *Phys. Today*, 2011, **64**, 31–36.

28 H. Jeffreys, *Math. Proc. Cambridge Philos. Soc.*, 1930, **26**, 204–205.

29 J. Seiwert, PhD thesis, Ecole Polytechnique X, 2010.

30 M. Maleki, M. Reyssat, F. Restagno, D. Quéré and C. Clanet, *J. Colloid Interface Sci.*, 2011, **354**, 359–363.

31 B. V. Derjaguin, *Prog. Surf. Sci.*, 1993, **43**, 134–137.

32 E. Rio and F. Boulogne, *Adv. Colloid Interface Sci.*, 2017, **247**, 100–114.

33 H. W. Krenn, J. D. Plant and N. U. Szucsich, *Arthropod Struct. Dev.*, 2005, **34**, 1–40.

34 C. J. Harper, S. M. Swartz and E. L. Brainerd, *PNAS*, 2013, **110**, 8852–8857.